

Novel Sampling Scheme on the Sphere for Head-Related Transfer Function Measurements

Alice P. Bates, *Student Member, IEEE*, Zubair Khalid, *Member, IEEE*, and Rodney A. Kennedy, *Fellow, IEEE*

Abstract—This paper presents a novel sampling scheme on the sphere for obtaining head-related transfer function (HRTF) measurements and accurately computing the spherical harmonic transform (SHT). The scheme requires an optimal number of samples, given by the degrees of freedom in the spectral domain, for the accurate representation of the HRTF that is band-limited in the spherical harmonic domain. The proposed scheme allows for the samples to be easily taken over the sphere due to its iso-latitude structure and non-dense sampling near the poles. In addition, the scheme can be used when samples are not taken from the south polar cap region of the sphere as the HRTF measurements are not reliable in south polar cap region due to reflections from the ground. Furthermore, the scheme has a hierarchical structure, which enables the HRTF to be analyzed at different audible frequencies using the same sampling configuration. In comparison to the proposed scheme, none of the other sampling schemes on the sphere simultaneously possess all these properties. We conduct several numerical experiments to determine the accuracy of the SHT associated with the proposed sampling scheme. We show that the SHT attains accuracy on the order of numerical precision (10^{-14}) when samples are taken over the whole sphere, both in the optimal sample placement and hierarchical configurations, and achieves an acceptable level of accuracy (10^{-5}) when samples are not taken over the south polar cap region of the sphere for the band-limits of interest. Simulations are used to show the accurate reconstruction of the HRTF over the whole sphere, including unmeasured locations.

Index Terms—2-sphere (unit sphere), head-related transfer function (HRTF) measurements, sampling, spectral analysis, spherical harmonic transform, spherical harmonics.

I. INTRODUCTION

THE head-related transfer function (HRTF) contains spatial information used by the listener to locate the source of sound and is used in the synthesis of binaural sound [1]–[9]. The HRTF is the ratio of the sound produced by a source to the sound received at the eardrum of a listener; it quantifies how

sound waves traveling in a particular direction are altered by interactions with the listener's head and torso before reaching the eardrum. Therefore, the knowledge of the HRTF for a particular individual enables the illusion of a spatially localized sound to be created [8], [10], [11]. The HRTF measurements in the audible frequency range ([0.2,20] kHz) are obtained by placing speakers (or microphones [12]) on a surrounding sphere in the far-field of the head (of a human subject or KEMAR mannequin) at a pre-defined set of longitudes and latitudes [2], [13]–[16] (see [13] for details of the different experimental set-ups used to obtain HRTF measurements).

In order to accurately determine the spectral domain representation of the HRTF and generate (or reproduce) the spatially localized sound, it is important to determine sample positions on the sphere that sufficiently capture the information contained in the HRTF. For a particular frequency, the HRTF at a constant distance (radius) from the listener is defined on the sphere. Therefore, the HRTF can be represented in the spectral domain characterized by spherical harmonics—the natural orthonormal basis functions on the sphere [17]. The spatial variation in the HRTF can be captured by a finite number of spherical harmonic coefficients by choosing a sufficiently large band-limit in the spectral domain characterized by spherical harmonics, where the band-limit is proportional to audible frequency [15], [18]. The spectral domain representation ensures the validity of the HRTF at unmeasured locations [13], [19], which is not theoretically guaranteed by other HRTF estimation methods (e.g., spline-based interpolation methods [19]). In practice, the spectral domain representation is obtained through the spherical harmonic transform (SHT) calculated numerically using a finite number of measurements of the HRTF made over the sphere [16]. Clearly, how the HRTF measurements are taken over the sphere is an important research question; the sampling scheme should allow the accurate computation of the SHT.

In addition to the numerical accuracy, a sampling scheme for acquiring HRTF measurements should allow for a number of practical considerations; it is desirable that the number of samples used in the scheme, defined as the spatial dimensionality of the scheme, be as small as possible [16], [20]. The HRTF measurements should be stored in a hierarchical structure that allows for different audible frequencies to be analyzed using the same sampling configuration i.e., the position of speakers (or microphones) on the sphere can remain the same when obtaining HRTF measurements for all audible frequencies [16]. Furthermore, it is also desirable that the scheme has an iso-latitude and/or iso-longitude structure, and non-dense sampling near the poles [16]. Another practical consideration that needs to be taken into account in the design of the measurement scheme is that the HRTF measurements from the large south polar cap

Manuscript received September 07, 2014; revised January 21, 2015; accepted March 25, 2015. Date of publication April 03, 2015; date of current version April 15, 2015. This work was supported by the Australian Research Council's Discovery Projects funding scheme under Project DP150101011. The associate editor coordinating the review of this manuscript and approving it for publication was Dr. Rongshan Yu.

A. P. Bates and R. A. Kennedy are with the Research School of Engineering, College of Engineering and Computer Science, The Australian National University, Canberra, ACT 2601, Australia (e-mail: alice.bates@anu.edu.au; rodney.kennedy@anu.edu.au).

Z. Khalid is with the Department of Electrical Engineering, University of Engineering and Technology, Lahore 54890, Pakistan (e-mail: zubair.khalid@uet.edu.pk).

Color versions of one or more of the figures in this paper are available online at <http://ieeexplore.ieee.org>.

Digital Object Identifier 10.1109/TASLP.2015.2419971

region of the sphere are often not taken, or are unreliable, because of ground reflections. Also, when designing a sampling scheme, it should be considered that the precise placement of speakers (or microphones) may not be possible in practice [14].

Many research groups have proposed different sampling schemes on the sphere to obtain the HRTF measurements [5], [6], [14], [16], [18], [19], [21]–[23]. However, none of the schemes simultaneously support accurate computation of the SHT and take into account all the practical requirements. With the consideration of the practical requirements identified from the experimental set-up and signal processing aspects, such as smaller spatial dimensionality, hierarchical and iso-latitude/iso-longitude structure, and non-dense sampling near the poles, the IGL00 sampling scheme [24] on the sphere has been favorably proposed in [16] for taking HRTF measurements, in comparison with the other schemes such as the equiangular scheme [25], [26], HEALPix (hierarchical equal-area iso-latitude pixelization) scheme [27] and Gauss-Legendre (GL) quadrature based scheme [28]. However, the IGL00 scheme only allows for the approximate computation of the SHT, where the approximation improves with a larger number of samples. We note that the HEALPix scheme, primarily developed for cosmological applications [27], although satisfies a number of practical requirements, only supports approximate computation of the SHT [16]. On the other hand, the equiangular and GL-quadrature based schemes [25], [26], [28] which support the accurate computation of the spherical harmonics require dense sampling near the poles. Furthermore, these schemes [26], [28] require twice the optimal number of samples, given by the degrees of freedom required to represent HRTF in spectral domain. Regularised least squares methods, such as the spherical microphone array for beamforming [14], do not allow for accurate SHT computation and are computationally intensive.

Recently, the optimal dimensionality scheme proposed in [20] enables the accurate computation of the SHT using the optimal number of samples and has non-dense sampling near the poles. However, the scheme does not have a hierarchical structure. Finally, we note that the existing schemes, with the exception of [14] do not allow for measurements not being taken from a potentially large south polar cap region. Later in the paper (in Section III), we summarize the requirements for the sampling scheme on the sphere for acquiring HRTF measurements, review the existing schemes in detail and identify that none of the existing schemes meet all of the requirements.

In this work, we aim to develop a sampling scheme on the sphere for taking HRTF measurements that achieves the optimal spatial dimensionality, allows for the accurate and fast computation of the SHT of the HRTF and also takes into account other practical considerations. To summarize, our main contributions in this work are:

- We propose an optimal sampling scheme on the sphere for acquiring measurements of HRTF with band-limited representation in spectral domain. The proposed scheme is hierarchical, consists of iso-latitude rings of samples with the flexibility in the placement of samples along longitude, allows for samples to be taken in the spatially-limited region (that excludes the south polar cap), does not require dense

samples near poles and achieves the optimal spatial dimensionality, given by the degrees of freedom required to represent band-limited HRTF in spectral domain.

- In the design of the sampling scheme, we develop a method to determine the placement of iso-latitude rings such that the SHT can be computed efficiently and accurately. Thus the proposed scheme and associated SHT enables valid and accurate representation of HRTF.
- We extensively study the accuracy of the SHT associated with the proposed sampling scheme for reconstructing any band-limited signal on the sphere and show that the SHT is accurate, with reconstruction error on the order of the numerical precision (10^{-14}), for the case when samples are taken over the whole sphere. For the samples taken over the spatially limited region, the proposed scheme also provides sufficient accuracy, with error on the order of 10^{-5} , for the band-limits associated with the representation of the HRTF in the audible frequency range ([0.2,20] kHz).
- The reconstruction of the HRTF using synthetic measurements, obtained from the spherical head model [29], is then carried out to show that the proposed method allows for accurate reconstruction of the HRTF over the whole sphere, including unmeasured locations, if a large enough band-limit is used.

The remainder of the paper is organized as follows. The necessary mathematical background and notation required to understand this work are contained in Section II. In Section III, the requirements of a sampling scheme for taking HRTF measurements and previous sampling schemes are discussed in greater detail. The proposed sampling scheme and SHT is presented in Section IV. In Section V, we evaluate the proposed scheme in terms of the requirements for an HRTF sampling scheme. Section VI contains synthetic experiments to objectively evaluate the accuracy of the proposed scheme in the reconstruction of the HRTF. Finally, concluding remarks are made in Section VII.

II. MATHEMATICAL PRELIMINARIES

In order to clarify the adopted notation, we present the necessary mathematical background for signals defined on the sphere and their spectral domain representation. We also briefly review the representation of the HRTF on the sphere.

A. Signals on the Sphere

Let $f(\theta, \phi)$ denote a square integrable complex function on the unit sphere denoted by \mathbb{S}^2 . The angles co-latitude $\theta \in [0, \pi]$ and longitude $\phi \in [0, 2\pi)$, where co-latitude is the angle from the positive z -axis and longitude is the angle from the positive x -axis in the x - y plane (Fig. 1), parameterize a point $(\sin \theta \cos \phi, \sin \theta \sin \phi, \cos \theta)' \in \mathbb{R}^3$ on \mathbb{S}^2 . The inner product of two functions $f(\theta, \phi)$ and $g(\theta, \phi)$ defined on \mathbb{S}^2 is given by [17]

$$\langle f, g \rangle \triangleq \int_{\mathbb{S}^2} f(\theta, \phi) \overline{g(\theta, \phi)} \sin \theta d\theta d\phi, \quad (1)$$

where $\overline{(\cdot)}$ denotes the complex conjugate and $\sin \theta d\theta d\phi$ is the differential area element on the sphere. The space of square integrable complex valued functions on \mathbb{S}^2 , equipped with the inner product in (1), forms a Hilbert space, denoted by $L^2(\mathbb{S}^2)$. The

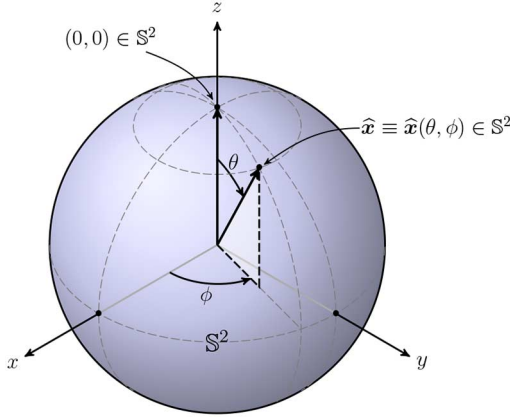


Fig. 1. Spherical co-ordinate system consisting of co-latitude θ and longitude ϕ parameterizes a point (θ, ϕ) on the unit sphere \mathbb{S}^2 .

inner product in (1) induces a norm $\|f\| \triangleq \langle f, f \rangle^{1/2}$. We refer to functions with finite induced norm as signals on the sphere.

B. Spherical Harmonics and Spectral Domain Representation

The Hilbert space $L^2(\mathbb{S}^2)$ is separable and spherical harmonic functions (spherical harmonics for short) form a complete orthonormal set of basis functions [17]. Spherical harmonics $Y_\ell^m(\theta, \phi)$ for integer degree $\ell \geq 0$ and integer order $|m| \leq \ell$ are defined as [17], [30]

$$Y_\ell^m(\theta, \phi) \triangleq \sqrt{\frac{2\ell+1}{4\pi} \frac{(\ell-m)!}{(\ell+m)!}} P_\ell^m(\cos\theta) e^{im\phi}, \quad (2)$$

where $P_\ell^m(\cdot)$ are the associated Legendre functions (with Condon-Shortley phase included) [17], [30].

Due to completeness of spherical harmonics, any signal $f \in L^2(\mathbb{S}^2)$ can be expanded using spherical harmonics as

$$f(\theta, \phi) = \sum_{\ell=0}^{\infty} \sum_{m=-\ell}^{\ell} (f)_\ell^m Y_\ell^m(\theta, \phi), \quad (3)$$

where $(f)_\ell^m$ denotes the spherical harmonic coefficient of degree ℓ and order m , and is calculated using the spherical harmonic transform (SHT), given by

$$(f)_\ell^m \triangleq \int_{\mathbb{S}^2} f(\theta, \phi) \overline{Y_\ell^m(\theta, \phi)} \sin\theta d\theta d\phi. \quad (4)$$

We note that the spherical harmonic coefficients $(f)_\ell^m$ form the spectral domain representation of the signal. We refer to the reconstruction of signal on the sphere from its spectral domain representation (spherical harmonic coefficients), given in (3), as the inverse SHT.

The signal $f \in L^2(\mathbb{S}^2)$ is said to be band-limited at degree L if $\forall \ell \geq L, |m| \leq \ell, (f)_\ell^m = 0$. The set of all band-limited signals forms a subspace of $L^2(\mathbb{S}^2)$ denoted by \mathcal{H}_L . For the expansion of band-limited signal $f \in \mathcal{H}_L$ using spherical harmonics, as given in (3), the summation over degree ℓ is truncated at $L-1$.

C. Head Related Transfer Function (HRTF)

The HRTF at a particular frequency and distance from the listener is naturally defined on the sphere. Let $H(\theta, \phi; k)$ denote the HRTF at a fixed distance from the listener with wavenumber $k = 2\pi f/c$, where f denotes the audible frequency and c is the

speed of sound propagation [15]. For each k , the HRTF can be represented as a band-limited function on the sphere and therefore can be expressed, using the inverse SHT, as

$$H(\theta, \phi; k) = \sum_{\ell=0}^{L(k)-1} \sum_{m=-\ell}^{\ell} (H)_\ell^m(k) Y_\ell^m(\theta, \phi), \quad (5)$$

where the spherical harmonic coefficients $(H)_\ell^m(k)$ are obtained using the SHT given by

$$(H)_\ell^m(k) = \int_{\mathbb{S}^2} H(\theta, \phi; k) \overline{Y_\ell^m(\theta, \phi)} \sin\theta d\theta d\phi. \quad (6)$$

The band-limit $L(k)$ is related to the wavenumber k (or frequency f) and the scattering object size s (typically the radius of the human head) through [15], [16]

$$L(k) \approx \left\lceil \frac{eks}{2} \right\rceil + 1 = \left\lceil \frac{e\pi s f}{c} \right\rceil + 1. \quad (7)$$

We note that the band-limit $L(k) = 47$ for maximum audible frequency $f = 20$ kHz [15], [16]¹. We further analyze the relation between the band-limit and the wavenumber given in (7) in Section VI-A.

III. HRTF ANALYSIS PROBLEM

A. Sampling Scheme Requirements

For the accurate spatial domain representation and spectral domain analysis of the HRTF, we are required to accurately determine the spherical harmonic coefficients given in (6) using the HRTF measurements. In addition to the numerical accuracy, a sampling grid designed for obtaining HRTF measurements should take into account a number of practical considerations [16], [24], [27]. For example, the number of sampling points, known as the spatial dimensionality, should be as small as possible, in order to reduce acquisition cost and time [13].

Since the number of spherical harmonic coefficients $(H)_\ell^m$ for the band-limited representation of HRTF $H(\theta, \phi; k)$ in (5) is $L(k)^2$, the optimal spatial dimensionality, denoted by N_O , attainable by any sampling scheme that supports accurate computation of the SHT is $N_O = L(k)^2$ [15]. Thus, in order to synthesise the HRTF over the entire audible frequency range, a minimum of $N_O = 47^2 = 2209$ samples are required. It is also desirable that a scheme does not require dense sampling near the poles to facilitate the acquisition of HRTF measurements near the poles [16], [24], [27]. The scheme should also have a hierarchical structure, with low spatial resolution data for lower audible frequency HRTF embedded in the high spatial resolution data that is used for HRTF with higher audible frequency, allowing for all frequencies in the audible range to be analyzed using the same sampling configuration [24], [27]. Since the experimental set-up to take HRTF measurements requires the rotation of either the sound source or receiver or both, it is desirable to have a scheme with an iso-latitude and/or iso-longitude structure as this results in the least number of rotations required to

¹Even if the effect of the torso is taken into consideration and its radius is used, the torso only contributes to the HRTF at frequencies less than 3 kHz and at frequencies above 3 kHz the radius, s , is that of the head [15], [31]. Hence the maximum band-limit, $L(k) = 47$, is valid for HRTF at all frequencies.

collect measurements. With these considerations, the sampling scheme on the sphere for HRTF measurements should satisfy the following requirements:

- (R1) Small spatial dimensionality
- (R2) Non-dense sampling at the poles
- (R3) Hierarchical structure of measurements
- (R4) Iso-longitude and/or iso-latitude
- (R5) Support an accurate SHT
- (R6) Efficient computation of the SHT

Moreover, we also take into account two more important practical considerations in the design of sampling scheme. First, we note that the precise placement of speakers (or microphones) along longitude may not be possible for obtaining HRTF measurements [32], [33]. If measurements are obtained one co-latitude at a time and the azimuth varied, as for the measurement procedure described in [33], then sample location accuracy is a problem around longitude, not co-latitude; it is therefore necessary to have a scheme where the location of samples is flexible along longitude. Second, the HRTF measurements are usually unavailable at elevations lower than about 140° due to ground reflections and limitations of the measurement apparatus [2], [15]. Hence, it is also desirable that the sampling scheme allows for accurate computation of the SHT when samples are not taken from the south polar cap region ($\theta > 140^\circ$) of the sphere. We append these two practical requirements for the sampling scheme to the list:

- (R7) Flexibility in the placement of samples
- (R8) Allow sampling over the spatially limited region

The requirements (R1)–(R5) have been considered in [16] for the evaluation of different sampling schemes on the sphere. However, the sampling schemes for obtaining HRTF measurements have not been evaluated against the requirements (R6)–(R8) in the existing literature.

B. Prior Work

In the literature, many sampling schemes on the sphere have been proposed for the analysis and the acquisition of measurements of the HRTF (e.g., [5], [6], [14], [16], [18], [19], [21]–[23]). In [16] four sampling schemes: equiangular grid, GL sampling, HEALPix and IGL00, were compared against four of the requirements, (R1)–(R4), listed in Section III-A. Here we evaluate schemes that allow analysis of the HRTF using spherical harmonics, including those mentioned above, against the eight listed requirements (R1)–(R8) to determine the suitability of the schemes for taking HRTF measurements.

We first consider the equiangular and GL quadrature based schemes, which support exact computation of the SHT of a signal on the sphere band-limited at L . Driscoll and Healy proposed an exact method to compute the SHT exploiting an equiangular sampling scheme, which consists of $2L$ equiangular spaced iso-latitude rings, where each ring consist of $2L - 1$ sample points along longitude. Thus, the spatial dimensionality of the Driscoll and Healy sampling scheme is approximately $4L^2$ points. Instead of placing $2L$ rings along longitude, the GL quadrature on the sphere [28], [34] can be used to develop a sampling scheme on the sphere that requires

L iso-latitude rings, where the placement of rings is dictated by the roots of Legendre polynomials of degree L . Recently, McEwen and Wiaux, through periodic extension of a sphere to a torus, proposed an equiangular sampling scheme and associated exact SHT, which also requires L iso-latitude equiangular spaced rings. It is noted that the spatial dimensionality for both the McEwen and Wiaux, and GL quadrature based sampling schemes is on the order of $2L^2$, with the McEwen and Wiaux scheme requiring $2(L - 1)$ fewer samples than the GL quadrature based scheme. Due to the iso-latitude and iso-longitude nature of the equiangular and GL quadrature based schemes, less rotations of the source and/or receiver are required for obtaining HRTF measurements than schemes that do not possess this property. Also, the iso-latitude structure in these schemes enables the efficient computation of the SHT through a separation of variables approach [25], [35]. In these schemes, the $2L - 1$ samples in each iso-latitude ring are equally spaced, which allows for the fast Fourier transform (FFT) to be used for efficient computation of the SHT. If the samples along each ring are not equally spaced, the SHT can also be computed accurately using the non-uniform discrete Fourier transform (NDFT) instead of the FFT, as long as the number of samples is $2L - 1$. Thus, these schemes could offer flexibility in the placement of samples along longitude in each ring. However, these schemes have a major drawback that they require dense sampling at the poles and hence are not commonly used for measuring HRTFs. We note that the equiangular sampling schemes satisfy the requirements (R4)–(R7), but fail to satisfy the first three requirements (R1)–(R3). It can be observed that the equiangular schemes are not fully hierarchical in nature as the sampling along co-latitude does not consist of the same sample point locations for different spatial resolutions. Among the equiangular and GL quadrature based schemes, the McEwen and Wiaux equiangular sampling scheme is most suitable for HRTF measurement as it has the smaller spatial dimensionality.

We also review the HEALPix² [27] and IGL00³ [24] sampling schemes which compute the SHT using approximate quadrature. The HEALPix scheme consists of sample points obtained by partitioning the sphere into equal surface area subregions [27]. It has been noted in [16] that the HEALPix scheme only meets the requirements (R2) and (R3). The IGL00 scheme is derived from the equiangular sampling method but, unlike the equiangular method, the IGL00 scheme can be used to achieve near equal-area division with no dense sampling near the poles [24]. Although iso-longitude sampling occurs in subregions, the IGL00 sampling scheme is not iso-longitude over the whole sphere. The IGL00 scheme can also be hierarchical, although there is a trade-off between the hierarchy and pixel distortion which affects the accuracy of the SHT. The IGL00 scheme with 12 base regions and 3:6:3 equal-area division configuration offers the best compromise between pixel distortion and hierarchy [24]. For the detailed comparison of the IGL00 scheme with the HEALPix and equiangular schemes, we refer the reader to

²<http://HEALPix.jpl.nasa.gov/>

³<http://www.mrao.cam.ac.uk/projects/cpac/igloo/>

TABLE I
COMPARISON OF DIFFERENT SAMPLING SCHEMES ON THE SPHERE FOR OBTAINING HRTF MEASUREMENTS

| | IGLOO | HEALPix | Gauss -Legendre | Equiangular (McEwen & Wiaux) | Beamforming Grid (Li and Duraiswami) | Optimal Dimensionality | Proposed |
|----------------------------------|-------|---------|--------------------|---------------------------------|---|---------------------------|----------|
| Number of Samples, $L=47$ | 3072 | 12288 | 4371 | 4279 | 2209 | 2209 | 2209 |
| Dense Sampling at Poles | No | No | Yes | Yes | Yes | No | No |
| Hierarchical | Yes | Yes | No | No | No | No | Yes |
| Iso-latitude/Iso-longitude | Yes | Yes | Yes | Yes | No | Yes | Yes |
| Accurate SHT | No | No | Yes | Yes | No | Yes | Yes |
| Computationally Efficient SHT | Yes | Yes | Yes | Yes | No | Yes | Yes |
| Flexibility in Samples Placement | No | No | Yes | Yes | Yes | No | Yes |
| Spatially Limited Sampling | No | No | No | No | Yes | No | Yes |

[16], where it has been reported that the IGL00 scheme is the most suitable scheme for HRTF measurement and analysis as it satisfies the requirements (R1)–(R4). We note that the IGL00 scheme, although supports the efficient computation (requirement (R6)) of the SHT through a separation of variables, has an associated SHT that is not accurate. Furthermore, the spatial dimensionality of the IGL00 scheme is not related to the HRTF band-limit, L and using a larger spatial dimensionality results in a greater accuracy of the SHT. The spatial dimensionality of the IGL00 scheme is larger than N_O , even when the reconstruction error (the error between measured HRTF and synthesized HRTF) is of the order 10^{-1} [16].

A number of sampling schemes used in HRTF analysis use least squares to calculate the spherical harmonic coefficients. In [14], Li and Duraiswami propose a flexible spherical grid for the design of spherical microphone array for beamforming, herein referred as beamforming grid. This beamforming grid requires the optimal number of points N_O , allows for flexibility in the placement of samples and spatially limited sampling. However it does not meet any of the other requirements; the structure of the grid is irregular, therefore not iso-longitude or iso-latitude and may have dense sampling at the poles [16]. In [19], regularised least squares is used to calculate the spherical harmonic coefficients on open grids (where samples are not taken over the whole sphere), which allows the reconstruction of HRTF with an accuracy within 5% of the ground truth data. Furthermore, the regularised least squares method of computing spherical harmonics only allows approximate computation of the spherical harmonic coefficients and is also computationally intense; least squares has computational complexity $O(L^6)$.

Recently a scheme which has optimal spatial dimensionality N_O and supports accurate computation of the SHT has been developed [20]. The scheme requires L iso-latitude rings and only $2n + 1$, $n = 0, 1, \dots, L - 1$, samples along each ring. However, the optimal dimensionality scheme does not meet requirements (R3), (R7) or (R8). Out of the existing sampling schemes, only that proposed by Li and Duraiswami has been designed to allow for spatially limited sampling, with samples not being taken over the south pole region. We summarize the comparison of different sampling schemes in Table I, where the number of samples required for each scheme for the maximum audible frequency of 20 kHz (corresponding to the band-limit $L = 47$) is shown. The number of samples for the HEALPix and IGL00 schemes are reported in [16] and result in reconstruction errors on the order of

10^{-4} and 10^{-1} respectively. If a band-limit $L > 47$ is used, in order accurately represent HRTF, the number of samples increases for all of the sampling schemes that allow accurate computation spherical harmonic transform.

C. Problem Statement and Contributions

In summary, there exists sampling schemes on the sphere, which satisfy some of the desired properties for HRTF measurement, the equiangular scheme of McEwen and Wiaux, the IGL00 and the optimal dimensionality schemes in particular. However, to our knowledge, no scheme exists that meets all of the eight listed requirements. The main contribution of this paper is the design of a sampling scheme on the sphere for HRTF analysis which meets all of the eight requirements (R1)–(R8) listed earlier in Section III-A, as reported in Table I. For the proposed sampling scheme, we also develop a fast and accurate algorithm for the computation of the SHT.

IV. PROPOSED SAMPLING SCHEME AND SPHERICAL HARMONIC TRANSFORM

For HRTF analysis and reconstruction, we here propose a sampling scheme and develop the associated SHT. We then evaluate the proposed sampling scheme in terms of the orthonormality of the spherical harmonics evaluated over the proposed grid.

A. Proposed Sampling Scheme—Structure

We propose an iso-latitude sampling grid, denoted by $\mathcal{S}(L)$, where samples are taken over iso-latitude rings. The L locations along θ where the iso-latitude rings are placed are stored in the vector $\boldsymbol{\theta}$ defined as

$$\boldsymbol{\theta} \triangleq [\theta_0, \theta_1, \dots, \theta_{L-1}]^T. \quad (8)$$

The ring placed at each θ_n is composed of $2n + 1$ samples along longitude ϕ . Let ϕ^n denote a vector of $2n + 1$ sampling points along ϕ in the ring placed at each θ_n , where

$$\phi^n \triangleq [\phi_1^n, \phi_2^n, \dots, \phi_{2n+1}^n]. \quad (9)$$

The vectors $\boldsymbol{\theta}$ and ϕ^n describe the structure of the sampling scheme $\mathcal{S}(L)$. However, we have not yet presented the location of these sample points. The most intuitive and simple choice of sample locations is to place the rings of samples equally along θ , with the rings with more samples along ϕ placed nearer to the equator ($\theta = \pi/2$), and have the samples in each ring equally

spaced along ϕ [20]. As an example, Fig. 2 shows this simple sampling arrangement for a band-limit $L = 8$. Such a placement of samples does not result in a hierarchical sampling scheme, nor provide flexibility in choosing sample locations. We first develop the SHT and inverse SHT for the proposed structure of the sampling scheme. We later provide details about the placement of the samples, that is, we design the vectors $\boldsymbol{\theta}$ and $\boldsymbol{\phi}^n$ for each $n = 0, 1, \dots, L - 1$ such that the sampling scheme meets the requirements (R1)–(R8).

B. Spherical Harmonic Transform

We here present a SHT⁴ to compute the spherical harmonic coefficients $(f)_\ell^m$ of a signal f band-limited at L and sampled over the sampling grid $\mathfrak{S}(L)$.

For order $|m| < L$, we define an indexed vector $\boldsymbol{\theta}^m \subset \boldsymbol{\theta}$ as

$$\boldsymbol{\theta}^m \triangleq [\theta_{|m|}, \theta_{|m|+1}, \dots, \theta_{L-1}]^T, \quad (10)$$

which consists of the last $L - |m|$ points in the vector $\boldsymbol{\theta}$.

By defining a vector

$$\mathbf{g}_m \equiv G_m(\boldsymbol{\theta}^m) \triangleq [G_m(\theta_{|m|}), G_m(\theta_{|m|+1}), \dots, G_m(\theta_{L-1})]^T, \quad (11)$$

with

$$\begin{aligned} G_m(\theta_n) &\triangleq \int_0^{2\pi} f(\theta_n, \phi) e^{-im\phi} d\phi \\ &= \int_0^{2\pi} \sum_{\ell=0}^{L-1} \sum_{m'=-\ell}^{\ell} (f)_\ell^{m'} Y_\ell^{m'}(\theta_n, \phi) e^{-im\phi} d\phi \\ &= \int_0^{2\pi} \sum_{\ell=0}^{L-1} \sum_{m'=-\ell}^{\ell} (f)_\ell^{m'} \tilde{P}_\ell^{m'}(\theta_n) e^{im'\phi} e^{-im\phi} d\phi \\ &= 2\pi \sum_{\ell=m}^{L-1} (f)_\ell^m \tilde{P}_\ell^m(\theta_n), \end{aligned} \quad (12)$$

for each order $|m| < L$ and each $\theta_n \in \boldsymbol{\theta}$, where

$$\tilde{P}_\ell^m(\theta_n) \triangleq Y_\ell^m(\theta_n, 0) = \sqrt{\frac{2\ell+1}{4\pi} \frac{(\ell-m)!}{(\ell+m)!}} P_\ell^m(\cos \theta_n), \quad (13)$$

denotes scaled associated Legendre functions, and a matrix \mathbf{P}_L^m as

$$\mathbf{P}_L^m \triangleq 2\pi \begin{pmatrix} \tilde{P}_{|m|}^m(\theta_{|m|}) & \tilde{P}_{|m|+1}^m(\theta_{|m|}) & \cdots & \tilde{P}_{L-1}^m(\theta_{|m|}) \\ \tilde{P}_{|m|}^m(\theta_{|m|+1}) & \tilde{P}_{|m|+1}^m(\theta_{|m|+1}) & \cdots & \tilde{P}_{L-1}^m(\theta_{|m|+1}) \\ \vdots & \vdots & \ddots & \vdots \\ \tilde{P}_{|m|}^m(\theta_{L-1}) & \tilde{P}_{|m|+1}^m(\theta_{L-1}) & \cdots & \tilde{P}_{L-1}^m(\theta_{L-1}) \end{pmatrix}, \quad (14)$$

a vector \mathbf{f}_m composed of spherical harmonic coefficients with order $|m| < L$

$$\mathbf{f}_m = [(f)_{|m|}^m, (f)_{|m|+1}^m, \dots, (f)_{L-1}^m]^T, \quad (15)$$

⁴We follow the formulation of the SHT presented in [20].

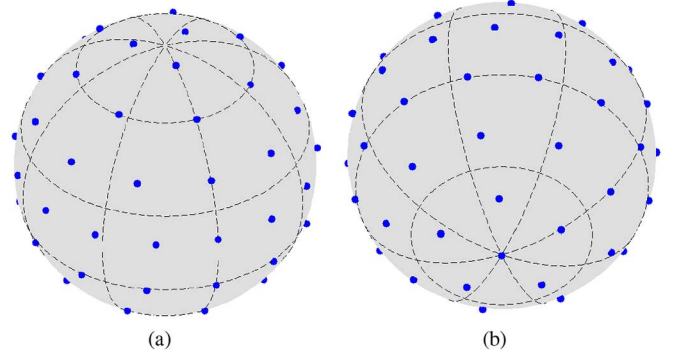


Fig. 2. Simple sampling arrangement for measuring a signal on the sphere band-limited at $L = 8$ (a) north pole view (b) south pole view.

can be computed by inverting the system

$$\mathbf{g}_m = \mathbf{P}_L^m \mathbf{f}_m, \quad (16)$$

for each $|m| < L$.

Using the formulation of the system in (16), the spherical harmonic coefficients of order $|m| < L$ contained in a vector \mathbf{f}_m can be computed accurately, provided the following two prerequisites are satisfied [20]:

- (P1) \mathbf{g}_m or equivalently $G_m(\theta_n)$ given in (12) for each $\theta_n \in \boldsymbol{\theta}^m$ is accurately computed
- (P2) $\boldsymbol{\theta}^m$ must be chosen such that \mathbf{P}_L^m can be accurately inverted

For the placement of samples in the proposed scheme $\mathfrak{S}(L)$, we use these conditions as guidelines to design $\boldsymbol{\theta}$ given in (8) and $\boldsymbol{\phi}^n$ given in (9) for all $n = 0, 1, \dots, L - 1$.

C. Inverse Spherical Harmonic Transform

The inverse SHT computes the signal from its spherical harmonic coefficients. Using the separation of variables technique, changing the order of summation in (3) and using (12), the inverse SHT can be expressed as

$$f(\theta, \phi) = \frac{1}{2\pi} \sum_{m=-(L-1)}^{L-1} e^{im\phi} G_m(\theta), \quad (17)$$

where $G_m(\theta)$ is given in (12). For the proposed sampling scheme, the inverse SHT can be computed by adopting the inverse SHT procedure proposed in [20].

D. Proposed Sampling Scheme—Design

For each $\theta_n \in \boldsymbol{\theta}^m$, the univariate signal $f(\theta_n, \phi)$ along ϕ can be made band-limited at $|m| + 1$, given the complex exponentials $e^{im\phi}$ as basis functions along ϕ [20]. Since there are at least $2m + 1$ number of points in each of the rings placed at $\theta_n \in \boldsymbol{\theta}^m$, $G_m(\theta_n)$ can be computed *accurately* (prerequisite P1) by evaluating the integral in equation (12) as a summation using the NDFT. If the samples along ϕ are equally spaced, that is,

$$\boldsymbol{\phi}^n = [0, \Delta_n, 2\Delta_n, \dots, (2n)\Delta_n], \quad \Delta_n = \frac{2\pi}{2n+1}. \quad (18)$$

the FFT can be used to compute $G_m(\theta)$ for each $\theta_n \in \boldsymbol{\theta}^m$.

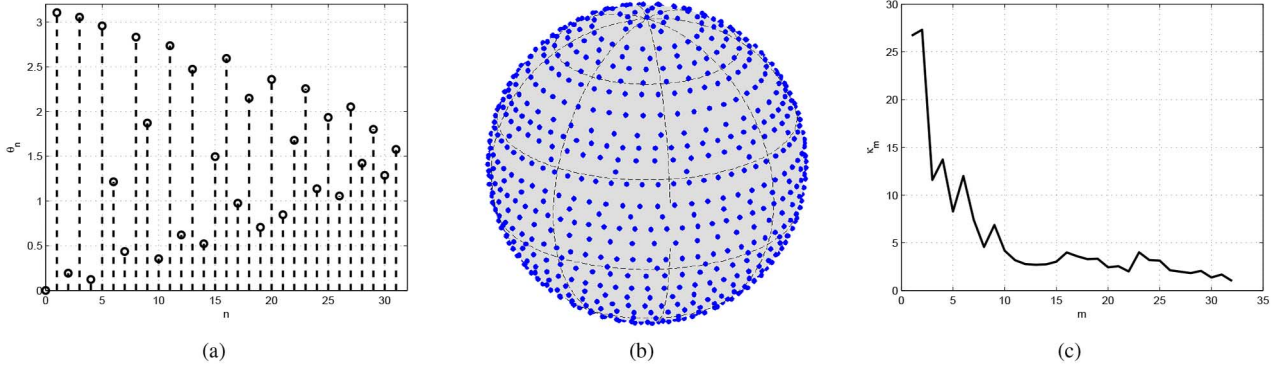


Fig. 3. (a) Sample positions $\theta_n \in \boldsymbol{\theta}$ obtained by applying steps 1 to 4 of the optimal sample placement method for $L = 32$ and $\theta_c = \pi$ (b) samples on the sphere and (c) the condition number κ_m of the matrix \mathbf{P}_L^m for $0 \leq m < L$.

In addition to accurately computing $G_m(\theta)$, we also require $\boldsymbol{\theta}^m$ to be chosen such that \mathbf{P}_L^m is well-conditioned in order for the accurate computation of the SHT (prerequisite P2). This places a constraint on the location of the rings along θ . Furthermore, we also consider that the samples along co-latitude to be taken over $\theta \in [0, \theta_c]$, which indicates that the samples are not taken over the south polar cap region of central angle $(\pi - \theta_c)$. When $\theta_c = \pi$, the samples are taken over the whole sphere. Therefore, we have two parameters in the design of sampling scheme; the band-limit L and θ_c specifying the sampling region. In order to choose L sample positions along co-latitude, we iteratively construct the vector $\boldsymbol{\theta}$ given in (8). We assume that we have $M \gg L$ equally spaced points along co-latitude over $\theta \in [0, \theta_c]$ ⁵. Since the ring at $\theta_0 \in \boldsymbol{\theta}$ contains only one sample, the natural choice to place such a ring is $\theta_0 = 0$ (north pole). We then choose θ_1 from given M points such that the condition number (ratio of the largest eigenvalue to the smallest eigenvalue) of the matrix \mathbf{P}_L^0 is minimized. Similarly, we choose $\theta_2, \theta_3, \dots, \theta_{L-1}$. Once we determine L samples along co-latitude, we use the condition number minimisation method [20] to reorder these L samples to form a vector $\boldsymbol{\theta}$ such that the matrix \mathbf{P}_L^m for each $|m| < L$ becomes better-conditioned. We refer to this procedure as the optimal samples placement method, which is summarized as follows:

- Step 1: Choose $M \gg L$ equiangular spaced points along co-latitude over $\theta \in [0, \theta_c]$.
- Step 2: Set $\theta_0 = 0$.
- Step 3: For each $z = 1, 2, \dots, L - 1$, choose such θ_z from the remaining $M - 1$ samples, which minimizes the condition number of the matrix \mathbf{P}_L^z .
- Step 4: Apply the condition number minimization method [20] to reorder the L sample points along co-latitude to form a vector $\boldsymbol{\theta}$.

Step 3 is used to select L locations in a vector $\boldsymbol{\theta}$ along co-latitude (for the placement of L iso-latitude rings) by ensuring that the $L \times L$ matrix \mathbf{P}_L^0 , which depends on all of $\theta_n \in \boldsymbol{\theta}$, is well-conditioned. This is a particularly important step for the sampling configuration when the samples are not taken over the whole sphere. Step 4 is then carried out to ensure that the matrix \mathbf{P}_L^m is well-conditioned for each order $0 \leq m < L$. Step 4 is necessary as the associated Legendre functions are close to zero

⁵If measurements are unavailable at some locations along θ , then these can be excluded from the M points available.

around the poles for large m , so it is more likely that the \mathbf{P}_L^m matrices may become ill-conditioned for large m [20].

As an illustration, we obtain the sample points by carrying about the above four steps for $L = 32$ and $\theta_c = \pi$ (whole sphere). The sample points along co-latitude in a vector $\boldsymbol{\theta}$ are shown in Fig. 3(a) along co-latitude and in Fig. 3(b) over the sphere. The condition number κ_m of the matrix \mathbf{P}_L^m constructed using samples for different values of $0 \leq m < L$ is plotted in Fig. 3(c). The condition number of each of the matrices \mathbf{P}_L^m is small, that enables the accurate computation of the SHT. We analyze the accuracy achieved by the proposed sampling later in the paper. We note that the optimal value of samples in a vector $\boldsymbol{\theta}$ using the proposed optimal samples placement method are required to be computed once only for each L and each θ_c . Once computed, $\boldsymbol{\theta}$, which describes the structure of the proposed sampling scheme $\mathfrak{S}(L)$, can be stored for use in the computation of the SHT.

E. Proposed Sampling Scheme—Orthonormality Error Analysis

Here we briefly study the accuracy of the proposed SHT; detailed accuracy analysis is carried out in the next section. We conduct a numerical experiment to validate the orthonormality relation $\langle Y_\ell^m(\theta, \phi), Y_{\ell'}^{m'}(\theta, \phi) \rangle = \delta_{\ell\ell'} \delta_{mm'}$. In our experiment, we generate the spherical harmonic function $Y_\ell^m(\theta, \phi)$ on the grid $\mathfrak{S}(L)$ and compute the spherical harmonic transform to determine the spherical harmonic coefficients $(Y_\ell^m)_{\ell'}^{m'}$ for each $\ell < L, |m| \leq \ell$ and $\ell' < L, |m'| \leq \ell'$. We compute the orthonormality error $E_{\text{ortho}}(\ell, m; \ell', m')$, defined as

$$E_{\text{ortho}}(\ell, m; \ell', m') \triangleq (Y_\ell^m)_{\ell'}^{m'} - \delta_{\ell\ell'} \delta_{mm'}, \quad (19)$$

for all $\ell < L, |m| \leq \ell$ and $\ell' < L, |m'| \leq \ell'$ and $L = 47$ (the band-limit that corresponds to the maximum audible frequency of 20 kHz). The orthonormality error is plotted as $\log_{10}(E_{\text{ortho}}(\ell, m; \ell', m'))$ in Fig. 4(a) and Fig. 4(b) for $\theta_c = \pi$ (samples over whole sphere) and $\theta_c = 0.8\pi$ (samples are taken over a spatially limited region that excludes the south pole), respectively. It can be observed that orthonormality errors are much smaller in comparison to the schemes that have an approximate SHT, indicating that the proposed scheme will permit higher reconstruction accuracy. For example, the IGLOO scheme has orthonormality errors on the order of 10^{-2} and 10^{-1} for the samples taken over the whole sphere and over the spatially limited region respectively [16].

V. ANALYSIS OF PROPOSED SAMPLING SCHEME AND SPHERICAL HARMONIC TRANSFORM

In this section we evaluate the proposed sampling scheme and associated SHTs against the requirements (R1)–(R8). We implement the proposed SHT in MATLAB. In order to speed up the computation, the three term recursion relation [20], [35], [36] is implemented in C language to compute the scaled associated Legendre function $\tilde{P}_\ell^m(\theta) \equiv Y_\ell^m(\theta, 0)$ for given θ , ℓ and m . We note that the three term recurrence relation, adopted here, that grows with degree ℓ for each m and θ is a natural choice for our implementation since we are required to compute the matrix \mathbf{P}_L^m for each m .

A. Number of Points

The total number of samples in the proposed sampling scheme are

$$\sum_{n=0}^{L-1} (2n+1) = L^2 = N_O, \quad (20)$$

which also represents the number of coefficients required for the representation of band-limited HRTF in the spectral domain. Thus, the sampling scheme $\mathfrak{S}(L)$ has the optimal spatial dimensionality, attainable by any sampling scheme that supports accurate computation of the SHT.

B. Non-dense, Hierarchical, Iso-latitude Sampling Scheme

By design, the samples in the proposed sampling scheme $\mathfrak{S}(L)$, characterized by θ and ϕ^n , respectively given in (8) and (9), do not partition the sphere into equal-area regions. However, the proposed scheme does not require significant dense sampling near the poles as compared to the equiangular sampling schemes [25], [26].

Furthermore, the proposed sampling scheme can be made fully hierarchical. The SHT of a band-limited signal at some degree $L' < L$ can be computed by taking the $(L')^2$ number of measurements over the higher resolution sampling scheme $\mathfrak{S}(L)$. For the computation of the SHT of a signal band-limited at some degree $L' < L$, we determine the L' ring positions θ_n for $n = 1, 2, \dots, L'$ from the scheme $\mathfrak{S}(L)$ designed for $L > L'$ with the consideration that (i) the ring at θ_n in the scheme $\mathfrak{S}(L)$ at least contains $2n+1$ sample points along longitude and (ii) each θ_n is chosen closest to the ring of $2n+1$ sample points along longitude in the grid $\mathfrak{S}(L')$. Once the L' rings are chosen from the sampling scheme $\mathfrak{S}(L)$, the $2n+1$ points along longitude in the ring placed at each θ_n are chosen such that the samples are maximally spaced. We note that samples over the rings $\theta_0, \theta_1, \dots, \theta_{L'-1}$ are different from the samples in the sampling scheme $\mathfrak{S}(L')$, optimally designed for band-limit L' . Therefore, the use of the higher resolution spatial grid $\mathfrak{S}(L)$ for obtaining the low resolution measurements of a signal band-limited at L' does not guarantee the accuracy of the SHT as the matrix $\mathbf{P}_{L'}^m$ may not be well-conditioned for each m . However, we later show that the SHT can be computed with sufficient accuracy for the band-limits in the range $0 \leq L \leq 64$ for the case when the hierarchical structure of the proposed sampling is exploited. Therefore, all frequencies in the audible frequency

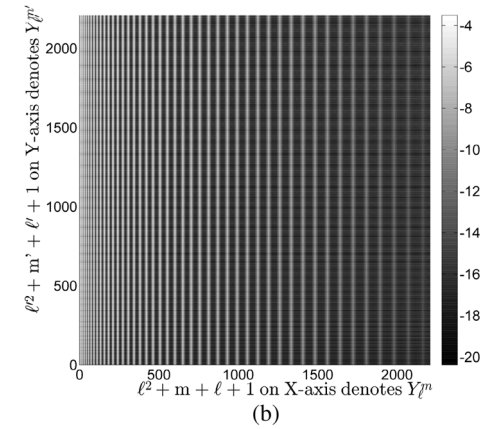
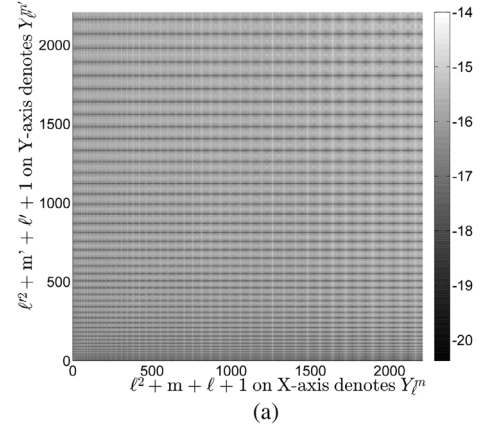


Fig. 4. Orthonormality error $E_{\text{ortho}}(\ell, m; \ell', m')$ (19) is plotted as $\log_{10}(E_{\text{ortho}}(\ell, m; \ell', m'))$ (a) over the whole sphere, $\theta_c = \pi$ and (b) over the spatially limited region $\theta_c = 0.8\pi$.

range ([0.2,20] kHz), corresponding to band-limits $L < 48$, can be analyzed using the same sampling configuration.

The proposed sampling scheme is naturally iso-latitude. This property allows HRTF measurements to be taken with fewer number of rotations of either the sounds source or human subject or both. Since the proposed sampling scheme does not restrict the samples in each ring to be equally spaced, the number of rotations can also be further reduced by placing the number of samples in each ring such that the samples along ϕ in different rings become iso-longitude.

C. Numerical Accuracy Analysis

The primary objective to design the sampling scheme on the sphere is to enable the computation of the SHT of the HRTF (a band-limited signal) from its measurements. The accuracy of the SHT is therefore the most important requirement. We carry out comprehensive accuracy analysis of the proposed sampling scheme and the associated SHT. We note that the analysis carried out in this section is valid for any band-limited signal on the sphere. In Section VI analysis is carried out on HRTF data so is only valid for the HRTF signal.

1) *Accuracy Test:* A sampling scheme is numerically accurate if the SHT of a band-limited signal followed by the inverse SHT results in an error between the original and resultant signal that is on the order of the numerical precision [20]. In order to evaluate the accuracy of the SHT associated with our sampling

scheme, we carry out the following experiment: we generate a complex valued band-limited test signal $f_T \in \mathcal{H}_L$ over the proposed sampling grid $\mathfrak{S}(L)$, where the complex value of each sample is randomly chosen with real and complex components from a uniform distribution on the interval $[-1, 1]$. The SHT followed by the inverse SHT is applied on the signal, resulting in the reconstructed signal f_R . We repeat this experiment 10 times and calculate the average values for the maximum and mean error between the original and reconstructed signal. The maximum reconstruction error E_{\max} and mean reconstruction error E_{mean} are defined as

$$E_{\max} \triangleq \max |f_T(\theta, \phi) - f_R(\theta, \phi)|, \quad (21)$$

$$E_{\text{mean}} \triangleq \frac{1}{L^2} \sum_{(\theta, \phi)} |f_T(\theta, \phi) - f_R(\theta, \phi)|. \quad (22)$$

2) *Sampling Scheme Configurations*: We carry out the numerical accuracy experiment for the band-limits in the range $8 \leq L \leq 64$ and for the following four different configurations of the sampling scheme:

- (C1) $\theta_c = \pi$; the samples along co-latitude are distributed over the whole sphere and samples along longitude in each ring are equally spaced as given in (18). Then the FFT can be used along iso-latitude samples in each ring to compute $G_m(\theta)$ given in (12).
- (C2) $\theta_c = \pi$; the samples along co-latitude are distributed over the whole sphere and samples along longitude in each ring are *not* equally spaced. As indicated earlier, the HRTF measurements may not be taken exactly at the longitude specified in (18); it is therefore necessary to analyze the accuracy of the proposed scheme with respect to variation in the sampling locations along longitude. Hence, we alter the sampling configuration used above, such that a small random component ϵ is added to the sample locations along longitude, ϕ_n , that is,

$$\tilde{\phi}^n \triangleq [\epsilon^n, \Delta_n + \epsilon^n, \dots, (2n)\Delta_n + \epsilon^n], \quad \Delta_n = \frac{2\pi}{2n+1}. \quad (23)$$

We take ϵ^n to be normally distributed with zero mean and standard deviation $\sigma_n = \frac{c}{2n+1}$, where $2n+1$ is the number of samples in a ring placed at θ_n and $c \in \mathbb{R}$ quantifies the standard deviation of sample locations from their designed location. Since the ring with fewer samples offers more flexibility in the placement of a sample away from its assigned location, we make the standard deviation σ_n inversely proportional to the number of samples in ring n .

- (C3) $\theta_c = \pi$; the samples along co-latitude are distributed over the whole sphere. The sampling grid $\mathfrak{S}(L)$ is created for a signal band-limited at $L = 64$. Samples for signals band-limited in the range $8 \leq L' \leq 64$ are then selected from this grid to form $\mathfrak{S}(L')$ as described in Section V-B. This configuration utilizes the hierarchical nature of the scheme.
- (C4) $\theta_c = 0.8\pi$; the samples along co-latitude are distributed over the spatially limited region. For simplicity, the sam-

ples along longitude in each ring are equally spaced as given in (18).

3) *Results*: We carry out the numerical accuracy test for each of the four sampling configurations (C1–C4). Since NDFT is required to be used to compute $G_m(\theta)$ given in (12) for configuration (C2), in order to be consistent, the SHT is computed using the NDFT rather than the FFT for all of the four configurations. We record the max error E_{\max} and the mean error E_{mean} , given by (21) and (22), respectively.

The errors E_{\max} and E_{mean} are plotted in Fig. 5(a) for configuration (C1). Although the errors grow with band-limit L^6 , the errors are still on the order of numerical precision for band-limits $L \leq 64$. Furthermore, it can also be observed that the errors increase as the band-limit L increases due to the computational flow of the SHT which causes the reconstruction errors to accumulate as spherical harmonic coefficients are sequentially calculated, for $m = L-1, L-2, \dots, 0$ [20]. The errors E_{\max} and E_{mean} for configuration (C2) are plotted in Fig. 5(b) for standard deviations with constants $c = 0.5$ and $c = 1$. It is evident that the errors are on the order of numerical precision for $L \leq 64$. It can also be noted that a smaller standard deviation results in a more accurate computation of the SHT. This is due to the fact that the larger standard deviation increases the maximum distance between neighboring samples which results in the sampling (locally) at a rate less than the Nyquist rate. For the configuration (C3), where the sampling grid designed for $L = 64$ is used to obtain samples for calculating the SHT for $8 \leq L' \leq 64$, the errors E_{\max} and E_{mean} , plotted in Fig. 5(c), are slightly larger than the errors for configuration (C1) shown in Fig. 5(a), due to the samples not being optimally selected for band-limit L' . However, the errors are both on the order of numerical precision for all band-limits $L' \leq 64$.

For the configuration (C4), when the samples are not taken over co-latitude greater than $\theta_c = 0.8\pi$, the errors E_{\max} and E_{mean} are plotted in Fig. 6(a). As predicted from the results of the orthonormality error analysis in Section IV-E, it can be observed that the errors grow at a greater rate in comparison to the errors when samples are taken over the whole sphere (configurations (C1)–(C3)). This is because the \mathbf{P}_L^m matrices are not as well-conditioned when samples are taken from a spatially limited region on the sphere, which can be observed in Fig. 6(b), where we plot the maximum condition number $\max(\kappa_m)$ for configurations (C1) and (C4), which clearly shows that $\max(\kappa_m)$ is larger for the configuration (C1) than (C4). Nevertheless, the errors for the configuration (C4) are on the order of 10^{-5} , or smaller, for band-limits of interest in HRTF analysis ($L < 48$).

Our numerical accuracy analysis demonstrates that the proposed sampling scheme allows the computation of SHT of any band-limited signal on the sphere that has a band-limit L up to and beyond the band-limits commonly considered in HRTF analysis with sufficient accuracy for all of the configurations. If the HRTF is indeed band-limited then the proposed scheme will enable the HRTF to be accurately reconstructed over the

⁶It is expected for E_{\max} and E_{mean} to monotonically increase with L , however in Fig. 5 there are local minima and maxima present. This numerical artifact is a result of the two condition minimisation methods described in Section IV-D.

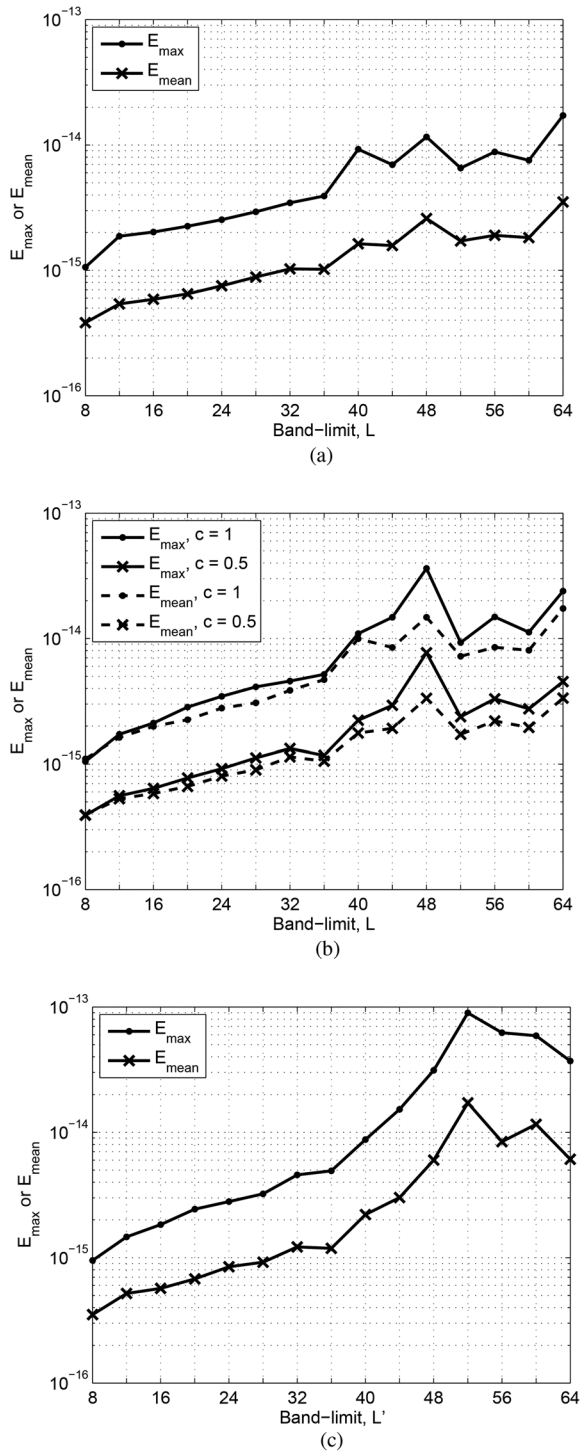


Fig. 5. Numerical accuracy analysis: plots of the maximum error E_{\max} and the mean error E_{mean} , respectively given in (21) and (22), for band-limits in the range $8 \leq L \leq 64$ and for the sampling configurations; (a) C1: $\theta_c = \pi$ and samples equally spaced around rings as given in (18), (b) C2: $\theta_c = \pi$ and samples not equally spaced around rings as given by (23) and (c) C3: $\theta_c = \pi$, L' rings taken from the ring locations in the sampling scheme designed for $L = 64$ for $8 \leq L' \leq 64$.

whole sphere. Thus, the proposed sampling scheme satisfies the requirements of allowing for flexibility in the placement of samples (R7), samples not being taken over the south polar cap region (R8) and having hierarchical structure (R3).

D. Computational Complexity Analysis

Here, we analyze the computational complexity of the SHT and inverse SHT for the proposed sampling scheme $\mathfrak{S}(L)$ designed to represent/measure the signal band-limited at L . Following the formulation of the SHT, we first compute \mathbf{g}_m for each m , which can be computed either using the FFT (when samples in each iso-latitude ring are equally spaced) or the NDFT, with complexity $O(L \log L)$ or $O(L^3)$ respectively. The matrix \mathbf{P}_L^m can be computed with complexity $O(L^2)$ for each m using the three term recurrence relation to compute the scaled associated Legendre function $\tilde{P}_\ell^m(\theta)$ [20]. The computation of \mathbf{f}_m requires solving the system in (16), which can be carried out naively using the least squares approach with complexity $O(L^3)$. However in practise, the system in (16) can be solved more efficiently by employing fast algorithms. For example, the system of size L can be solved in $O(L^{2.37})$, instead of $O(L^3)$, using the algorithm of [37]. These operations are required to be repeated for each m , which is of the order L , therefore, the complexities mentioned above are scaled by L and therefore the overall asymptotic complexity of the SHT transform scales as $O(L^4)$. The dominant factor $O(L^4)$ is due to the inverting of system in (16) and the use of the NDFT for the case when samples are not equally spaced around ϕ , which can be more efficiently implemented in practice [38], [39] and we demonstrate in this section that the complexity of the SHT transform scales close to $O(L^3)$ in practice. If the inverse matrices $(\mathbf{P}_L^m)^{-1}$ (or pseudo-inverse) for all $m < L$ and matrices required in the computation of the NDFT are pre-computed, the theoretical complexity reduces to $O(L^3)$. We note that the pre-computation of these matrices require storage of the order $O(L^3)$, which is manageable for the band-limits used in HRTF analysis. In our implementation of the SHT, we use on-the-fly computation of these matrices. Since the inverse SHT in (17) is formulated by exploiting the iso-latitude structure of the proposed sampling scheme that enables a separation of variables (contribution of complex exponentials along ϕ and associated Legendre functions along θ), the inverse SHT can be computed with computational complexity $O(L^3)$ [20].

We measure the computation time to carry out the proposed SHT for the configurations (C1) and (C2), where we use FFT and NDFT, respectively, to compute \mathbf{g}_m . The time taken to compute the SHT of the complex band-limited test signal f_T for band-limits $8 \leq L \leq 64$ is recorded and averaged over 10 test signals for each of the configurations (C1) and (C2). The experiment is performed using MATLAB running on a machine equipped with 3.4 GHz Intel Core i7 processor and 8 GB of RAM. The computation time in seconds, denoted by τ , for each configuration is plotted in Fig. 7, where it can be seen that τ for each configuration is always less than 1 second and scales closer to $O(L^3)$ than $O(L^4)$.

VI. EVALUATION OF PROPOSED SAMPLING SCHEME AND SPHERICAL HARMONIC TRANSFORM USING SPHERICAL HEAD MODEL

Here we evaluate the accuracy of our method for the reconstruction of the HRTF on the sphere. We use the spherical head model [29] to obtain synthetic HRTF data for the following parameters: head radius $a = 0.09$ m with measurements taken over a sphere at a distance of $r = 1$ m from the head. This model

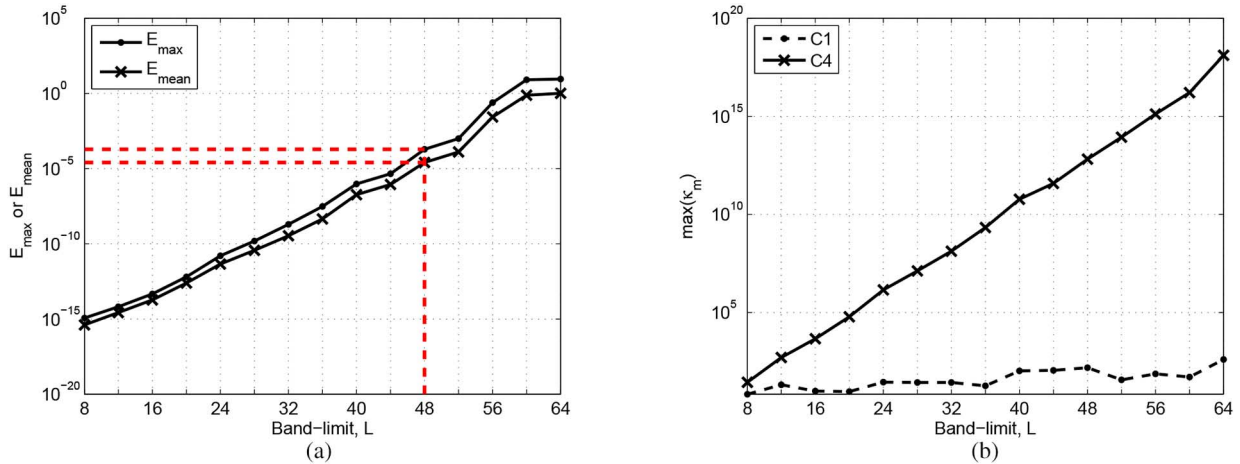


Fig. 6. (a) Plot of the maximum error E_{\max} and the mean error E_{mean} , respectively given in (21) and (22), for band-limits in the range $8 \leq L \leq 64$ for the sampling configuration (C4): $\theta_c = 0.8\pi$ and samples equally spaced around rings, and (b) the maximum of the condition number, $\max(\kappa_m)$, $0 \leq m < L$ for band-limits $8 \leq L \leq 64$ for configurations (C1) and (C4). Note that $\max(\kappa_m)$ is much larger for (C4) than for (C1). In (a) E_{\max} and E_{mean} for the maximum band-limit of interest in HRTF analysis ($L < 48$) are shown by the red dotted lines.

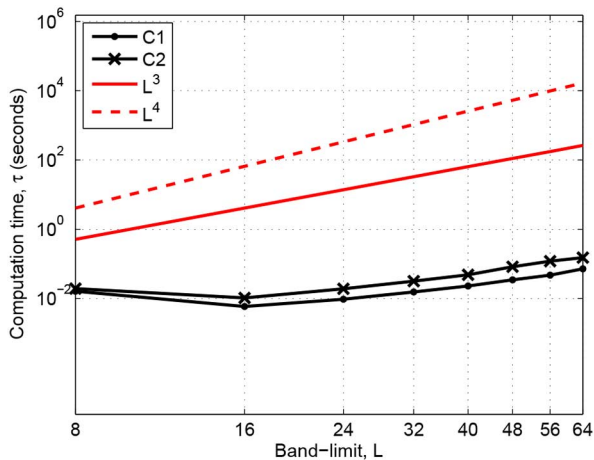


Fig. 7. The computation time τ in seconds to carry out the SHT for band-limits in the range $8 \leq L \leq 64$ and for the configurations (C1) and (C2), where we use the FFT and the NDFT, respectively, to determine \mathbf{g}_m in the computation of the SHT. Note that both scale closer to $O(L^3)$ than $O(L^4)$ due to the use of efficient techniques for inverting the matrix system. The $O(L^3)$ and $O(L^4)$ scaling is shown by solid and dashed red lines (without markers) respectively.

also requires a threshold level at which the spherical Hankel functions are calculated to be specified; we set the threshold at 10^{-15} (machine precision).

A. HRTF Band-limit Analysis

In the literature [1], [15], [18], the HRTF band-limit in the spherical harmonic basis is often taken to be given by (7) ($L(k) = \lceil \frac{e\pi s f}{c} \rceil + 1$, where the wavenumber k is directly proportional to frequency f), resulting in a maximum band-limit of $L = 47$ at the highest audible frequency $f = 20$ kHz. Since the proposed sampling scheme permits accurate computation of SHT of any band-limited signal as demonstrated in Section V-C, the proposed scheme will enable the HRTF to be accurately reconstructed over the whole sphere provided the HRTF is indeed band-limited. Before attempting to analyze the accuracy of the HRTF reconstruction, it is therefore important to verify that the signal is indeed band-limited as related by (7).

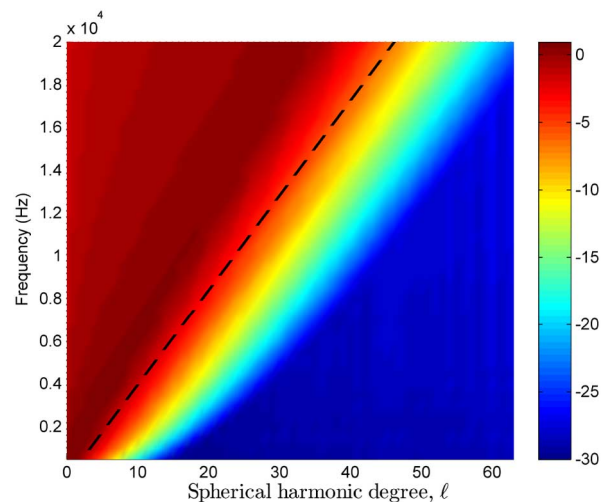


Fig. 8. The energy spectrum $S(f, \ell)$, given in (24), of the HRTF is plotted in logarithmic scale as $\log_{10} S(f, \ell)$ for spherical harmonic degrees $0 \leq \ell < 64$ and all frequencies f in the audible range. The black dashed line indicates the band-limit (maximum degree) $\ell = L(k)$ given in (7) as a function of wavenumber (or frequency).

In order to determine the band-limit of the synthetic HRTF, we compute the HRTF spherical harmonic coefficients $(H)_{\ell}^m(k)$ up to $L = 64$ from the synthetic measurements that are obtained using the spherical head model over the (C1) sampling configuration described in Section V-C2. For different frequencies over the audible range, we compute the energy spectrum $S(f, \ell)$, defined as

$$S(f, \ell) \triangleq \sum_{m=-\ell}^{\ell} |(H)_{\ell}^m(k)|^2, \quad \ell < L, \quad (24)$$

which is plotted in logarithmic scale in Fig. 8, where it is evident that the HRTF is indeed a band-limited function, with $S(f, \ell)$ becoming very small at higher degrees. We have also indicated the band-limited $L(k)$ given by (7) as dashed line in Fig. 8. Although the energy spectrum $S(f, \ell)$ decreases sharply after the band-limit given by (7), there is still considerable energy contributed by higher degree spherical harmonics. Therefore, using

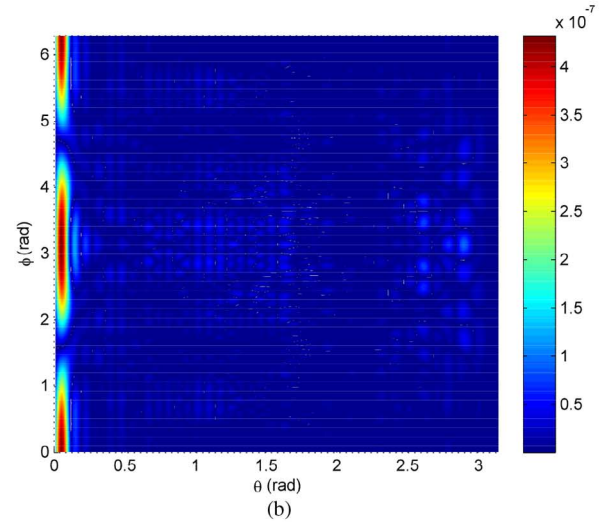
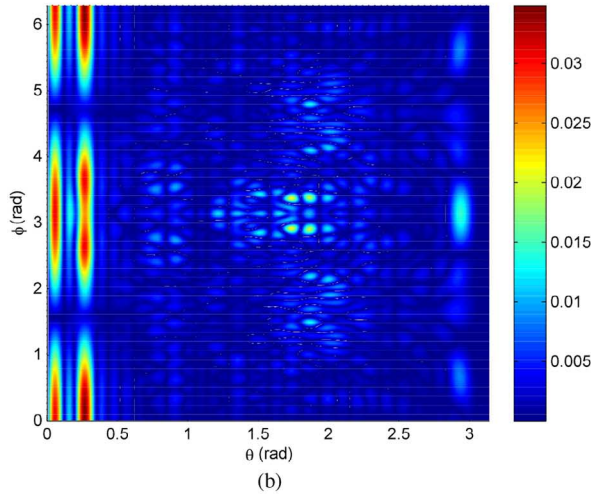
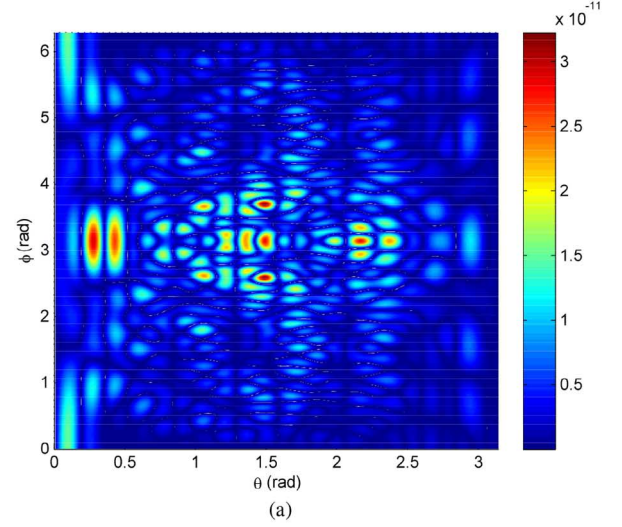
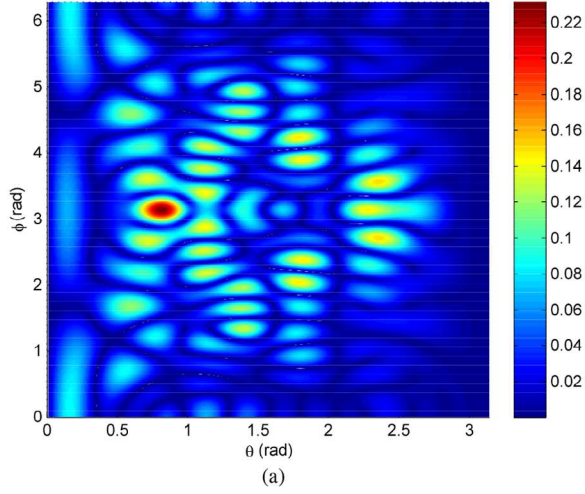


Fig. 9. Reconstruction error $E_R(\theta, \phi; k)$ given in (25) of the HRTF on the sphere at (a) $f = 5$ kHz with $L = 13$ and (b) $f = 15$ kHz with $L = 35$, where the band-limit is calculated using (7).

Fig. 10. Reconstruction error $E_R(\theta, \phi; k)$ given by (25) of the HRTF on the sphere using larger band-limits at (a) $f = 5$ kHz with $L = 28$ and (b) $f = 15$ kHz with $L = 47$.

the band-limit given by (7) will result in truncation error, which can be reduced by using a larger band-limit, as we demonstrate in the next section.

B. HRTF Reconstruction Accuracy Analysis

In order to evaluate the numerical accuracy of the proposed scheme in the reconstruction of the HRTF over the whole sphere, not just at locations where measurements have been obtained, we conduct a following experiment:

- For a given frequency f , synthetic measurements of the HRTF $H(\theta, \phi; k)$ are obtained over the sampling grid $\mathcal{S}(L)$ with (C1) sampling configuration described in Section V-C2.
- Compute spherical harmonic coefficients $(H)_m^\ell(k)$ using the proposed SHT.
- The spherical harmonic coefficients $(H)_m^\ell(k)$ are used to reconstruct the HRTF over a very high resolution equiangular grid (consisting of 197192 points).

We compute the error $E_R(\theta, \phi; k)$ between the reconstructed HRTF $H_R(\theta, \phi; k)$ and the analytical value of the HRTF $H_A(\theta, \phi; k)$ obtained from the spherical head model, given by

$$E_R(\theta, \phi; k) \triangleq |H_A(\theta, \phi; k) - H_R(\theta, \phi; k)|, \quad (25)$$

which is plotted in Fig. 9(a) and Fig. 9(b) for $f = 5$ kHz and $f = 15$ kHz, respectively. Here we have used $L = 13$ and $L = 35$ for $f = 5$ kHz and $f = 15$ kHz, respectively, as dictated by (7). We also determine the error $E_R(\theta, \phi; k)$, plotted in Fig. 10, for higher band-limits, that is, $L = 28$ and $L = 47$ for $f = 5$ kHz and $f = 15$ kHz, respectively. As expected from our above analysis of the HRTF band-limit, the reconstruction accuracy greatly improves with a higher band-limit, due to reduced truncation error. This demonstrates that the proposed scheme can be used to accurately reconstruct the HRTF over the entire sphere, provided that a suitable band-limit is used. Determining the suitable band-limit, that allows HRTF reconstruction to an accuracy on the order of numerical precision, is worth further investigation, however, is beyond the scope of this work. The

reconstruction error is of the same order of magnitude over the whole sphere, demonstrating that the proposed scheme allows sufficiently accurate interpolation of the HRTF at unmeasured locations.

VII. CONCLUSIONS

We have proposed a new sampling scheme on the sphere and developed a computationally efficient SHT for the accurate representation and spectral domain analysis of the HRTF. In comparison to the previous sampling schemes, we have shown that the proposed scheme satisfies all practical and processing requirements. The scheme attains optimal spatial dimensionality as it requires the optimal number of samples, that is equal to the number of degrees of freedom in harmonic space, for the accurate computation of the SHT. In addition, the proposed scheme is non-dense near the poles and is iso-latitude, allowing for the measurements to be more easily obtained. Furthermore, the proposed scheme can be configured as fully hierarchical which enables the HRTF to be analyzed at all frequencies in the audible range using the same arrangement of speakers (or microphones).

We have conducted numerical experiments to show the reconstruction accuracy of any band-limited signal on the sphere for band-limits of interest in HRTF analysis for four different configurations of the sampling scheme. Errors on the order of machine precision are obtained for the configurations where samples are taken over the whole sphere, demonstrating that the scheme allows for flexibility in the placement of samples along longitude and has a hierarchical structure. An acceptable reconstruction error can be obtained when samples are taken from a spatially limited region (excluding south polar cap region) on the sphere. We also show that the SHT can be carried out with manageable computational complexity. Simulations have been carried out to show that the proposed sampling scheme and SHT allows for accurate reconstruction of the HRTF over the whole sphere, including unmeasured locations, provided that a suitable band-limit is chosen. The future work includes the use of the proposed scheme for the acquisition of HRTF measurements and further investigation into improving the numerical accuracy for the configuration when samples on the sphere are not taken from the south polar cap region.

REFERENCES

- [1] D. N. Zotkin, R. Duraiswami, and N. A. Gumerov, "Sound field decomposition using spherical microphone arrays," in *Proc. IEEE Int. Conf. Acoust., Speech, Signal Process. (ICASSP'08)*, Las Vegas, NV, USA, Mar. 2008, pp. 277–280.
- [2] Y. Luo, D. N. Zotkin, H. Daume, and R. Duraiswami, "Kernel regression for head-related transfer function interpolation and spectral extrema extraction," in *Proc. IEEE Int. Conf. Acoust., Speech, Signal Process. (ICASSP'13)*, Vancouver, BC, Canada, May 2013, pp. 256–260.
- [3] T. Ajdler, C. Faller, L. Sbaiz, and M. Vetterli, "Sound field analysis along a circle and its application to HRTF interpolation," *J. Audio Eng. Soc.*, vol. 56, no. 3, pp. 156–175, Mar. 2008.
- [4] D. S. Brungart and G. D. Romigh, "Spectral HRTF enhancement for improved vertical-polar auditory localization," in *Proc. IEEE Workshop Appl. Signal Process. Audio Acoust.*, New Paltz, NY, USA, Oct. 2009, pp. 305–308.
- [5] G. Enzner, M. Krawczyk, F. M. Hoffmann, and M. Weinert, "3D reconstruction of HRTF-fields from 1D continuous measurements," in *Proc. IEEE Workshop Appl. Signal Process. Audio Acoust.*, New Paltz, NY, USA, Oct. 2011, pp. 157–160.
- [6] M. Pec, M. Bujacz, and P. Strumiłło, "Head related transfer functions measurement and processing for the purpose of creating a spatial sound environment," *Proc. SPIE*, vol. 6937, Jan. 2008.
- [7] R. Martin and K. McAnally, Interpolation of head-related transfer functions Air Operations Division Defence Science and Technology Organisation, Tech. Rep., Feb. 2007.
- [8] D. S. Talagala, W. Zhang, T. D. Abhayapala, and A. Kamineni, "Binaural sound source localization using the frequency diversity of the head-related transfer function," *J. Acoust. Soc. Amer.*, vol. 135, no. 3, pp. 1207–1217, 2014.
- [9] X. L. Zhong, F. C. Zhang, and B. S. Xie, "On the spatial symmetry of head-related transfer functions," *Appl. Acoust.*, vol. 74, no. 6, pp. 856–864, Jan. 2013.
- [10] Y. Luo, D. N. Zotkin, and R. Duraiswami, in *Statistical analysis of head-related transfer function (HRTF) data*, Montreal, QC, Canada, Jan. 2013, vol. 19, no. 1.
- [11] B. S. Xie, "Recovery of individual head-related transfer functions from a small set of measurements," *J. Acoust. Soc. Amer.*, vol. 132, no. 1, pp. 282–294, 2012.
- [12] D. N. Zotkin, R. Duraiswami, E. Grassi, and N. A. Gumerov, "Fast head-related transfer function measurement via reciprocity," *J. Acoust. Soc. Amer.*, vol. 120, no. 4, pp. 2202–2215, Oct. 2006.
- [13] G. D. Romigh, "Individualized head-related transfer functions: Efficient modeling and estimation from small sets of spatial samples," Ph.D. dissertation, Carnegie Mellon Univ., Pittsburgh, PA, USA, 2012.
- [14] Z. Li and R. Duraiswami, "Flexible and optimal design of spherical microphone arrays for beamforming," *IEEE Trans. Acoust., Lang., Signal Process.*, vol. 15, no. 2, pp. 702–714, Feb. 2007.
- [15] W. Zhang, T. D. Abhayapala, R. A. Kennedy, and R. Duraiswami, "Insights into head-related transfer function: Spatial dimensionality and continuous representation," *J. Acoust. Soc. Amer.*, vol. 127, no. 4, pp. 2347–2357, Apr. 2010.
- [16] W. Zhang, M. Zhang, R. A. Kennedy, and T. D. Abhayapala, "On high-resolution head-related transfer function measurements: An efficient sampling scheme," *IEEE Trans. Acoust., Lang., Signal Process.*, vol. 20, no. 2, pp. 575–584, Feb. 2012.
- [17] R. A. Kennedy and P. Sadeghi, *Hilbert Space Methods in Signal Processing*. Cambridge, U.K.: Cambridge Univ. Press, Mar. 2013.
- [18] C. D. Salvador Castaneda, S. Sakamoto, J. A. Trevino Lopez, J. Li, Y. Yan, and Y. Suzuki, "Accuracy of head-related transfer functions synthesized with spherical microphone arrays," in *Proc. ICA*, Montreal, QC, Canada, Jun. 2013, vol. 19, no. 1.
- [19] D. N. Zotkin, R. Duraiswami, and N. A. Gumerov, "Regularized HRTF fitting using spherical harmonics," in *Proc. IEEE Workshop Appl. Signal Process. Audio Acoust.*, New Paltz, NY, USA, Oct. 2009, pp. 257–260.
- [20] Z. Khalid, R. A. Kennedy, and J. D. McEwen, "An optimal-dimensionality sampling scheme on the sphere with fast spherical harmonic transforms," *IEEE Trans. Signal Process.*, vol. 62, no. 17, pp. 4597–4610, Sep. 2014.
- [21] K. Matsui and A. Ando, "Estimation of individualized head-related transfer function based on principal component analysis," *Acoust. Sci. Tech.*, vol. 30, no. 5, pp. 338–347, Feb. 2009.
- [22] M. J. Evans, J. A. S. Angus, and A. I. Tew, "Analyzing head-related transfer function measurements using surface spherical harmonics," *J. Acoust. Soc. Amer.*, vol. 104, no. 4, pp. 2400–2411, Jun. 1998.
- [23] Q. Huang and Y. Fang, "Interpolation of head-related transfer functions using spherical Fourier expansion," *Chinese J. Electron.*, vol. 26, no. 4, pp. 571–576, Jul. 2009.
- [24] R. G. Crittenden and N. G. Turok, "Exactly azimuthal pixelizations of the sky," *Arxiv preprint astro-ph/9806374*, 1998.
- [25] J. R. Driscoll and D. M. Healy, Jr., "Computing Fourier transforms and convolutions on the 2-sphere," *Adv. Appl. Math.*, vol. 15, no. 2, pp. 202–250, Jun. 1994.
- [26] J. D. McEwen and Y. Wiaux, "A novel sampling theorem on the sphere," *IEEE Trans. Signal Process.*, vol. 59, no. 12, pp. 5876–5887, Dec. 2011.
- [27] K. M. Górski, E. Hivon, A. J. Banday, B. D. Wandelt, F. K. Hansen, M. Reinecke, and M. Bartelmann, "HEALPix: A framework for high-resolution discretization and fast analysis of data distributed on the sphere," *Astrophys. J.*, vol. 622, pp. 759–771, Apr. 2005.
- [28] W. Skukowsky, "A quadrature formula over the sphere with application to high resolution spherical harmonic analysis," *J. Geodesy*, vol. 60, no. 1, pp. 1–14, Mar. 1986.
- [29] R. O. Duda and W. L. Martens, "Range dependence of the response of a spherical head model," *J. Acoust. Soc. Amer.*, vol. 104, no. 5, pp. 3048–3058, Nov. 1998.

- [30] J. J. Sakurai, *Modern Quantum Mechanics*, 2nd ed. Reading, MA, USA: Addison Wesley, 1994.
- [31] V. R. Algazi, C. Avendano, and R. O. Duda, "Elevation localization and head-related transfer function analysis at low frequencies," *J. Acoust. Soc. Amer.*, vol. 109, no. 3, pp. 1110–1122, Mar. 2001.
- [32] V. R. Algazi, R. O. Duda, D. M. Thompson, and C. Avendano, "The CIPIC HRTF database," in *Proc. IEEE Workshop Applicat. Signal Process. Audio and Acoust.*, New Paltz, NY, USA, 2001, pp. 99–102.
- [33] B. Gardner and K. Martin, "HRTF measurements of a KEMAR dummy-head microphone," MIT Media Lab Perceptual Computing, Tech. Rep., May 1994.
- [34] A. G. Doroshkevich, P. D. Naselsky, O. V. Verkhodanov, D. I. Novikov, V. I. Turchaninov, I. D. Novikov, P. R. Christensen, and Chiang, "Gauss legendre sky pixelization (GLESP) for CMB maps," *Int. J. Mod. Phys. D.*, vol. 14, no. 2, pp. 275–290, Feb. 2005.
- [35] D. M. Healy, Jr., D. Rockmore, P. J. Kostelec, and S. S. B. Moore, "FFTs for the 2-sphere - improvements and variations," *J. Fourier Anal. Appl.*, vol. 9, pp. 341–385, 2003.
- [36] P. J. Kostelec and D. N. Rockmore, "FFTs on the rotation group," *J. Fourier Anal. Appl.*, vol. 14, pp. 145–179, 2008.
- [37] D. Coppersmith and S. Winograd, "Matrix multiplication via arithmetic progressions," *J. Symb. Comput.*, vol. 9, no. 3, pp. 251–280, 1990.
- [38] A. Dutt and V. Rokhlin, "Fast Fourier transforms for nonequispaced data II," *Appl. Comput. Harmon. Anal.*, vol. 2, no. 1, pp. 85–100, 1995.
- [39] K. Gröchenig, "A discrete theory of irregular sampling," *Linear Algebra Appl.*, vol. 193, pp. 129–150, 1993.



Alice P. Bates (S'11) received a B.E. (First-Class Hons.) degree in electrical engineering from the University of Auckland, New Zealand, in 2013. She is currently working towards a Ph.D. from the Research School of Engineering, the Australian National University, Australia.

Ms. Bates received the Senior Scholar Award for first in her cohort during her undergraduate studies. She was also awarded an Australian Postgraduate Award for the duration of her Ph.D. Her research interests are related to the application driven devel-

opment of signal processing techniques for the collection and processing of signals with spherical geometry.



Zubair Khalid (S'10–M'13) received his B.Sc. (First-class Hons.) degree in electrical engineering from the University of Engineering & Technology (UET), Lahore, Pakistan, in 2008. He received the Ph.D. degree in engineering from the Australian National University of Canberra, Australia, in Aug. 2013.

He is currently working as an Assistant Professor in the Department of Electrical Engineering, University of Engineering and Technology, Lahore, Pakistan. Previously, he was working as a Research Fellow in the Research School of Engineering, Australian National University (ANU), Canberra, Australia. He was awarded University Gold Medal and Industry Gold Medals from Siemens and Nespak for his overall outstanding performance in Electrical Engineering during the his undergraduate studies. He was a recipient of an Endeavour International Postgraduate Award for his Ph.D. studies. His research interests are in the area of signal processing and wireless communications, including the development of novel signal processing techniques for signals on the sphere and the application of stochastic geometry in wireless ad-hoc networks.



Rodney A. Kennedy (S'86–M'88–SM'01–F'05) received the B.E. degree (1st class honours and university medal) from the University of New South Wales, Sydney, Australia, the M.E. degree from the University of Newcastle, and the Ph.D. degree from the Australian National University, Canberra. Since 2000, he has been is a Professor in engineering at the Australian National University, Canberra, Australia.

He has co-authored over 300 refereed journal or conference papers and a book *Hilbert Space Methods in Signal Processing* (Cambridge Univ. Press, 2013). He has been a Chief Investigator in a number of Australian Research Council Discovery and Linkage Projects. His research interests include digital signal processing, digital and wireless communications, and acoustical signal processing.